Nanoscale

Phonon induced near-field effects on heat transfer across nanogap electrodes

Journal:	*Nanoscale*
Manuscript ID	NR-ART-10-2024-004355.R1
Article Type:	Paper
Date Submitted by the Author:	15-Nov-2024

Complete List of Authors:	Hanamura, Yuki; Osaka University Graduate School of Engineering Science School of Engineering Science, Division of Frontier Materials Science Kishimoto, Kazuma; Osaka University Graduate School of Engineering Science School of Engineering Science, Division of Frontier Materials Science Tada, Mizuki; Osaka University Graduate School of Engineering Science School of Engineering Science, Division of Frontier Materials Science Yamada, Ryo; Osaka University Graduate School of Engineering Science School of Engineering Science, Division of Frontier Materials Science Tada, Hirokazu; Osaka University Graduate School of Engineering Science School of Engineering Science, Division of Frontier Materials Science

Journal Name

ARTICLE TYPE

Cite this: DOI: 00.0000/xxxxxxxxxx

Phonon induced near-field effects on heat transfer across nanogap electrodes†

Yuki Hanamura, Kazuma Kishimoto, Mizuki Tada, Ryo Yamada, and Hirokazu Tada*

Received Date
Accepted Date

DOI: 00.0000/xxxxxxxxxx

Heat transfer at the nanoscale remains largely unexplored compared to that in bulk materials, particularly phonon tunneling across extremely narrow nanogaps. The underlying mechanisms of this phenomenon are not well understood due to experimental difficulties. As a novel approach for measuring heat transfer in nanogaps, we have developed an on-chip adiabatic mechanically controllable break junction system based on a suspended membrane device. The electrical and thermal conductance were measured simultaneously across the gold nanogap, with the spacing controlled by a built-in actuator. Our results indicate anomalous thermal conductance at gap distances of a few nanometers, strongly suggesting phonon-mediated heat transfer in these extremely confined spaces.

1 Introduction

Nanomaterials exhibit remarkable characteristics in heat transfer, characterized by phenomena such as ballistic transport and quantized behavior. These unique characteristics arise from their constrained spatial structure impeding carrier diffusion.[1–6] In a nanoscale vacuum gap devoid of carrier materials, heat transfer occurs through electromagnetic waves within the infrared region. When the gap distance becomes comparable to the wavelength, the evanescent wave facilitates heat transfer, a phenomenon known as near-field radiative heat transfer (NFRHT).[7–12] This anomalous heat transfer phenomenon has sparked considerable interest, particularly for its applications across various fields including scanning thermal microscopy,[13] local cooling,[14] microfabrication through localized heating,[15] and enhancing the performance of solar cells.[16]

Recent investigations utilizing scanning tunneling microscopes with integrated thermometers have reported significant heat transfer in gaps narrower than a few nanometers.[17–19] Intriguingly, this considerable heat transfer cannot be fully elucidated by conventional NFRHT mechanisms. Theoretical models propose alternative mechanisms for transferring heat through electrons and phonons rather than solely electromagnetic waves.[20–26] While electrons may be transported via tunneling, phonons cannot exist in a vacuum, indicating that phonon transport across the gap seems counterintuitive. However, when the gap distance is sufficiently small, mechanical interactions between the electrodes, such as Coulomb and van der Waals forces, may cause vibrations of the atoms comprising the electrodes to propagate between them.[22–26] This vibrational propagation constitutes phonon transport, which transfers heat through the gaps. Since the electron tunneling decays rapidly as an exponential function of distance,[27] whereas the mechanical interactions decay slowly as a polynomial function,[22–24,26] phonon transport may occur at larger gap distances than electron transport. While such distance-dependent heat transfer specific to the heat carrier is theoretically expected, the correspondence between these theoretical frameworks and experimental observations remains largely unexplored, primarily due to the inherent challenges in precisely measuring heat transfer at the nanoscale. Research endeavors focused on bridging the gap between theoretical predictions and experimental observations possess considerable potential for uncovering novel insights into nanoscale heat transfer phenomena.

In the present work, we show a novel approach for quantifying the distance-dependent thermal conductance between nanogaps on a suspended membrane device. The suspended membrane device, initially pioneered by Kim *et al.*,[28] has evolved into a fundamental tool for measuring the thermal conductance of nanowires, as demonstrated by numerous studies.[29–36] We have engineered a device in which the gap distance can be precisely controlled by integrating an electro-thermal actuator into the suspended membrane structure. Similar to the mechanically controllable break junction method,[37–39] the actuator allowed the electrodes to contact and break repeatedly. This approach endowed the device with both controllability and thermal isolation, facilitating precise thermal conductance measurement across nanogaps while modulating the gap distance.

Graduate School of Engineering Science, Osaka University, Toyonaka 560-8531, Japan. E-mail: tada.hirokazu.es@osaka-u.ac.jp

† Electronic Supplementary Information (ESI) available: Details on the device preparation, measurements, and numerical simulations for data analysis. See DOI: 00.0000/00000000.

2 Methods

2.1 Device preparation

The device was prepared on a silicon substrate coated with a 100 nm-thick silicon nitride film. Metallic electrodes were constructed on the film using conventional electron beam lithographic techniques, followed by partial etching of the underlying substrate to form a suspended structure, as described in the ESI.† Fig. 1 (a) illustrates a schematic of the device, while Figs. 1 (b)-(d) show scanning electron microscope (SEM) images. In the center, highlighted in yellow in Fig. 1 (a), a nano-scale gap was created between the electrodes. On both sides, bridge-like structures were designed to accommodate a heater and a thermometer, shown in blue. Additionally, diagonal beams, highlighted in red, were devised to serve as electro-thermal actuators, enabling precise adjustment of the gap distance. When a voltage V_{act} was applied to the thin metal wires on the beams, they expanded, causing the entire suspended structure to deform and, thus reducing the gap distance. Conversely, decreasing the voltage V_{act} caused the beams to retract, allowing the electrodes to move apart again. The symmetric arrangement of the beams in an X-shaped pattern prevented the device from deforming during the wet etching process in its preparation by evenly distributing stresses. Due to the difficulties in reproducibly creating well-aligned nanogaps using lithographic techniques, we employed gold electroplating on submicroscale gap electrodes to increase their thickness and ensure sufficient contact surfaces. Fig. 1 (d) shows an enlarged view of a nanogap electrode prepared by electroplating. Further details on the preparation of nanogaps are provided in the ESI.†

2.2 Measurement of thermal conductance

To quantify the thermal conductance across the nanogap, we employed a method involving the application of an AC electrical current to the heater, while simultaneously utilizing a lock-in technique to monitor temperature fluctuations. The AC current, with an amplitude I_{ac} (= 150 μA) and an angular frequency ω, was applied to the heater-bridge, inducing a temperature wave oscillating at an angular frequency of 2ω and an amplitude of approximately 2 K. Leveraging the dependence of the heater's resistance on temperature, we obtained the heater's temperature by measuring the third harmonic component of the voltage $V_{3\omega}$. Concurrently, a portion of the heat $Q_{2\omega}$ generated at the heater propagated to the sensor-bridge, oscillating at the angular frequency 2ω. The sensor's temperature was determined by applying a DC current I_{dc} (= 100 μA) to the sensor and measuring the second harmonic component of the voltage $V_{2\omega}$. Further details on the measurement of harmonic voltage components and temperature derivation are provided in the ESI.† By measuring these temperatures, the thermal conductance κ of the nanogap can be determined using the following equation, commonly utilized for suspended membrane devices:[40–43]

$$\kappa = Q\frac{\Delta T_{\mathrm{s}}}{{\Delta T_{\mathrm{h}}}^2 - {\Delta T_{\mathrm{s}}}^2} \tag{1}$$

where Q is the heat generated solely at the heater, and ΔT_{h} and ΔT_{s} represent the amplitudes of the temperature oscillations of the heater and sensor, respectively. Since thermal resistances inside the device and the heat generated at the leads of the heater affect the actual measurements, a correction factor derived from numerical simulations was integrated into eqn (1). Details on the compensation of κ are provided in the ESI.† Although the actuators produce static heat, it does not affect the calculation of κ. This is because the heat is symmetrically generated on both bridges, and the lock-in measurement exclusively targets the oscillating heat flow. From the frequency response of the temperature oscillations, the thermal response time of the device (τ) was approximately 1.6 ms. We used a frequency $\omega/(2\pi) = 5$ Hz to measure κ in steady state, which is enough slow compared to $1/(2\pi\tau) \approx 100$ Hz. To deal with the time delay inherent to lock-in measurements with low-frequency signals, we used a custom-built data acquisition system rather than a commercial lock-in amplifier. In the ESI,† we have detailed the frequency characteristics of the device and the compensation for the time delay. All measurements were performed in a cryostat (Quantum Design, Inc., PPMS) at 300 K unless otherwise specified and under high vacuum ($< 10^{-3}$ Pa) to minimize heat transfer via convection from residual gas molecules[44].

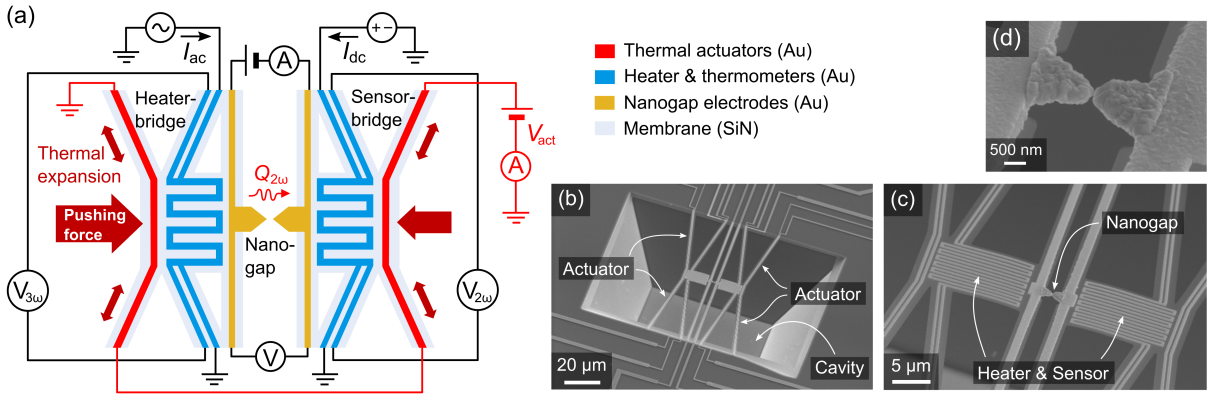

Fig. 1 (a) Schematic of the device and experimental setup, (b) SEM image of the device, (c) Enlarged view of thermal measuring part, and (d) Nanogap electrodes prepared by electroplating.

3 Results and discussion

3.1 Analysis of gap distance

Fig. 2 (a) shows the relationship between the applied power P to the actuator and the corresponding thermal conductance κ and electrical conductance G across the gaps as a function of elapsed time. The quantized conductance G_0 ($= 77.5\ \mu$S), representing the conductance of a single atomic chain of gold,[45,46] acts as the threshold for detecting electrode contact. Initially, P was gradually raised while a bias voltage V_b ($= 10$ mV) was applied across the gaps. Once the electrodes approached each other closely, tunneling current began to flow. As G surpassed 1 G_0, there was a sharp rise, indicating electrode contact. A rapid increase in κ was also observed when the electrodes made contact. P was then decreased to separate the electrodes. Plateaus of G in the contact regime suggest plastic deformation of gold electrodes. Following electrode breakage, increasing P facilitated re-contact, and this process could be repeated more than 100 times. During the breaking process, the contact electrodes were rapidly separated due to plastic deformation and self-breaking, and thus, tunneling currents could not be observed in some cases. Therefore, all measurements were performed during the approaching process of the electrodes, allowing their position to be monitored and controlled.

We evaluated the distance between the electrodes from the Simmon's formula.[27] The tunneling current J_T is described as follows when the bias voltage V_b is sufficiently small.

$$J_T = \frac{3\sqrt{2m\phi}S}{2d}\left(\frac{e}{h}\right)^2 V_b \exp\left[-\frac{4\pi d}{h}\sqrt{2m\phi}\right] \quad (2)$$

Here m represents the effective mass of electron, ϕ the work function of electrode, S the cross-sectional area of the electrode, d the distance between gaps, e the elementary charge, and h the Planck constant. Assuming that the displacement of d is proportional to the thermal expansion of the actuator, i.e. the power input to the actuator, the following equation is derived.

$$d = \alpha(P_C - P) \quad (3)$$

where α represents the coefficient of thermal expansion concerning the power consumption of the actuator, and P_C denotes the power applied when the gap contacts. This assumption is consistent with the results of the numerical simulations as described in the ESI.† By combining eqns (2) and (3), the electrical conductance G can be obtained using the following expression:

$$G = \frac{A}{\alpha(P_C - P)}\exp\left[-\alpha B(P_C - P)\right] \quad (4)$$

where A and B are constants defined as $A = 3e^2\sqrt{2m\phi}S/(2h^2)$ and $B = 4\pi\sqrt{2m\phi}/h$, respectively. Since A and B are known once the values of ϕ and S are experimentally determined, the parameter α can be obtained by fitting the values of G and P to eqn (4). Fig. 2 (b) shows the fitting result in the regime where the tunneling current increases as the electrode approach each other. For this fitting, ϕ was determined to be 3.9 eV by fitting eqn (2) to the relationship of J_T versus V_B when the gap distance was kept constant, as shown in the inset graph of Fig. 2 (b). The surface area S was determined to be 50 nm × 50 nm based on SEM observations, as shown in the inset SEM image of Fig. 2 (b). From

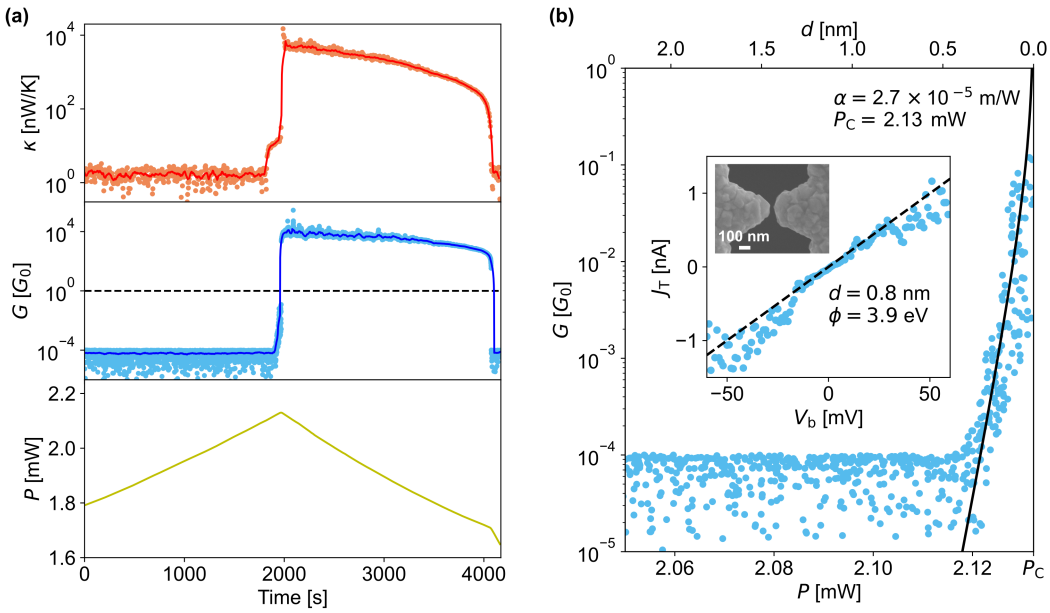

Fig. 2 (a) Plots of thermal conductance κ, electrical conductance G, and applied power to the actuator P as a function of time. Circular markers represent data points, while the central lines denote the moving average of the data. (b) Estimation of the gap distance d by fitting the values of G and P to eqn (4). The fitting was performed in the regime where $P > 2.12$ mW ensuring the tunneling current exceeded the noise floor. The fitting result is shown as a black line. The inset plot shows the tunneling current J_T as a function of the bias voltage V_B with a constant gap distance where the black dashed line represents the fit according to eqn (2). An inset SEM image depicts the nanogap electrode used for the measurement.

these results, α was obtained to be $(2.7 \pm 0.7) \times 10^{-5}$ m/W.

The upper scale shown in Fig. 2 (b) represents the estimated d using the obtained α and eqn (3). Although the Simmon's formula supposes planar electrodes and is not appropriate for electrodes with sharp geometries, the estimated d is on the scale of a few nanometers, and the contact surface of the electrode, which is on the order of 1000 nm^2, can be considered sufficiently large and flat.

Note that the temperature around the gap electrodes increased by approximately 50 K due to the Joule heat generated at the actuators, even though the substrate temperature was maintained at 300 K. However, at the gap electrodes close to the nanoscale discussed in this study, the actuator is almost fully expanded, and its temperature fluctuations are slight. In addition, the device was heated not only by the actuator but also by a heater for thermal conductance measurement. Although the thermal expansion of the heater and its leads might modulate the gap distance, the power dissipation of the heater was approximately AC 10 μW, which is roughly two orders of magnitude smaller than that of the actuator. Furthermore, the lock-in measurement smoothed the thermal conductance values, making the slight fluctuations of the electrodes negligible.

3.2 Distance dependence of thermal conductance

Fig. 3 shows the changes in thermal conductance κ and electrical conductance G as a function of the gap distance d with the substrate temperature maintained at 300 K. κ was measured while sweeping the gap distance at a rate of 0.003 $\sim$ 0.01 nm/s, which was slow enough compared to τ, enabling the observation of κ against d with sub-nanometer resolution. When the gap distance exceeded a certain threshold ($d > 1.5$ nm), κ remained nearly constant, indicating a regime dominated by radiative heat transfer. In the gold electrodes, since surface plasmon polaritons cannot be excited at near room temperatures,[26] their contribution to heat transfer is negligible. Thus, the radiation contribution can be attributed solely to electromagnetic waves oscillating in the out-of-plane direction of the electrode, which converges to a constant thermal conductance as the gap distance approaches the nanometer scale.[26] Our experimental results were consistent with these theoretical predictions. On the other hand, a sharp increase in κ occurred within the extremely close vicinity ($d < 1.5$ nm). Since the energy $J_T V_b$ transferred by tunneling electrons was over two orders of magnitude smaller than the heat flow measured in this regime, the contribution of electrons to heat transfer was negligible. As the magnitude of the gap distance approached the regime where phonon-mediated heat transfer was theoretically anticipated, thermal conductance induced by phonons was expected to be proportional to $d^{-2.7} \sim d^{-3.2}$ according to the theories.[21–26] In our results, the rising edge of κ was approximately proportional to d^{-5}. This deviation from theoretical predictions could be attributed to the geometry and surface roughness introduced during the preparation, while most theories assume atomically flat electrodes. Note that the behavior of κ was consistently reproducible across nanogaps prepared using the same procedure. However, we observed a different trend ($\kappa < d^{-2.1}$) for a nanogap

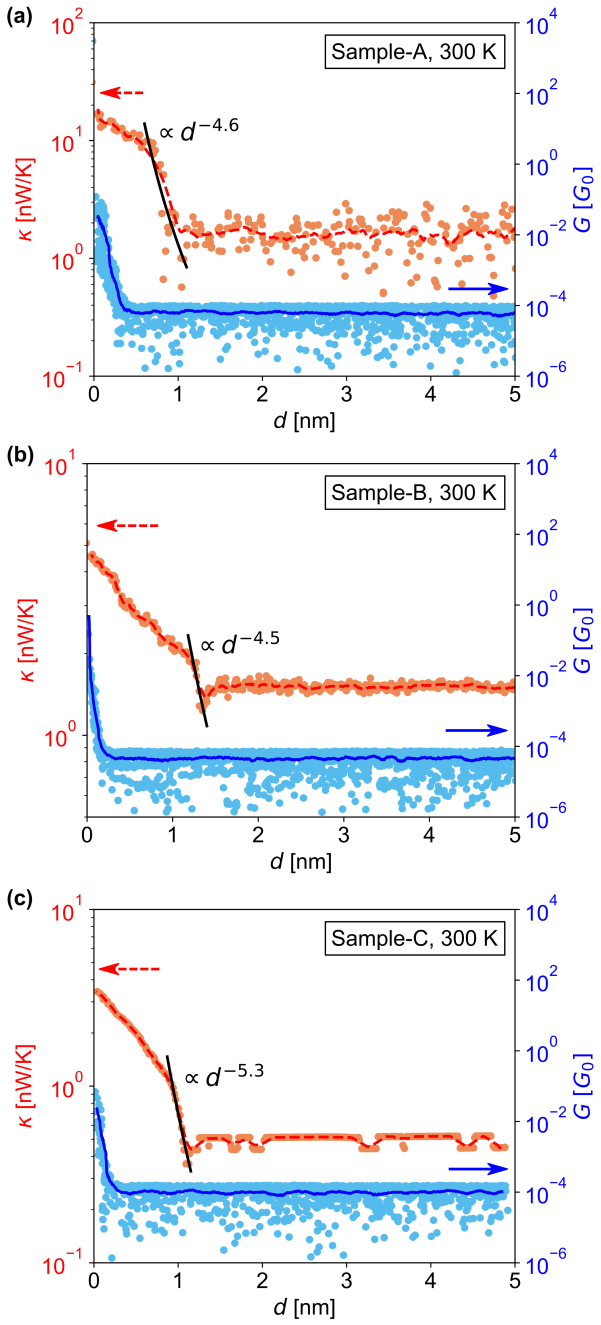

Fig. 3 Distance dependence of thermal conductance κ (red, left axis) and electrical conductance G (blue, right axis) for the electroplated gold nanogaps. The labels (a)-(c) denote that the data were obtained from different samples. The variation in the signal-to-noise ratio of κ among the samples can be attributed to differences in the input range of the lock-in measurement and the gap distance sweep rate.

without electroplating, as shown in the ESI.† These results suggested that phonon transport is strongly affected by the shape and atomic configuration inherent to the electrode tip. In each result, κ showed an inflection point with respect to d, indicating the involvement of multiple forces in phonon transport. For example, when the gap electrodes were far apart, Coulomb and van der Waals forces acted as attractive forces and enhanced each other. In contrast, at extremely close distances, van der Waals

forces became repulsive, canceling the attractive Coulomb force and potentially reducing phonon transport. After the electrodes made contact, we observed an increase in κ due to electron transport, as shown in Fig. 2 (a). These experimental findings provide evidence for the transition of primary heat carriers from radiation to phonons and electrons, depending on the distance between the nanogap.

3.3 Temperature dependence of thermal conductance

If phonons dominate heat transfer across the nanogap, a decrease in the temperature of the electrodes should reduce phonon density and consequently decrease thermal conductance. Fig. 4 shows the distance dependence of thermal and electrical conductance across the nanogap when the device was cooled. The labels (a) and (b) correspond to the measured results at substrate temperatures of 100 K and 50 K, respectively. While anomalous increases in κ were observed even at low temperatures, the slope of the rising part of κ was steeper than that at 300 K. The heat transfer due to tunneling electrons was expected to show $d^{-10.2} \sim d^{-12.6}$ manner,[26] suggesting that the electron contribution became more dominant than that of phonons as the temperature decreased. In addition, the rising edge of κ approached $d = 0$ as the temperature decreased with the regime of increased κ overlapping the tunneling conduction regime, indicating the significant contribution of electrons to heat transport. These findings provide further evidence for phonon transport across the nanogaps around 300 K, as observed in Fig. 3.

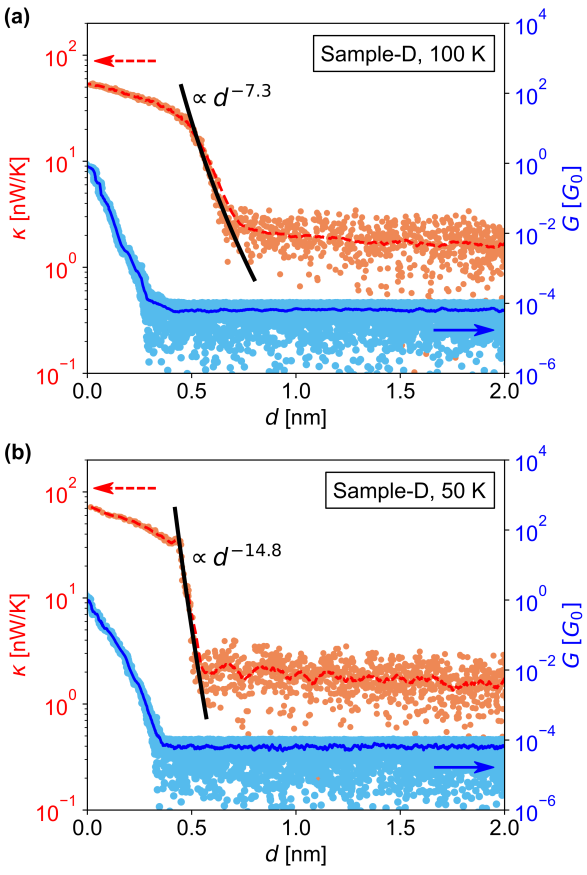

Fig. 4 Distance dependence of thermal conductance κ (red, left axis) and electrical conductance G (blue, right axis) at ambient temperatures of (a) 100 K and (b) 50 K.

Conclusions

In summary, we have constructed a suspended membrane device equipped with a built-in actuator for measuring the thermal conductance of gold nanogaps. Our measurements of thermal conductance across a broad spectrum of gap distances have unveiled the distinct contributions of radiation, phonons, and electrons to heat transfer. Notably, the anomalous thermal conductance observed in a few nanometer gaps strongly indicates the presence of the near-field effects in heat transfer, facilitated by phonon transport resulting from mechanical interactions between the electrodes.

Author contributions

Yuki Hanamura: methodology, investigation, formal analysis, data curation, and writing – original draft. Kazuma Kishimoto: investigation, formal analysis and data curation. Mizuki Tada: investigation, formal analysis and data curation. Ryo Yamada: supervision, project administration, and writing – review & editing. Hirokazu Tada: conceptualization, supervision, funding acquisition, project administration, and writing – review & editing.

Conflicts of interest

There are no conflicts to declare.

Data availability

The data supporting this article have been included as part of the ESI.†

Acknowledgements

This work was supported by JSPS KAKENHI Grant Numbers 18H03899, 22H00315 and 23K17903 and JST SPRING, Grant Number JPMJSP2138. A part of this work was conducted in Advanced Research Infrastructure for Materials and Nanotechnology Open Facilities in Osaka University, supported by ARIM Program of MEXT, Japan, Grant Number JPMXP1224OS1032. The SEM images were obtained at the Analytical Instrument Facility, Graduate School of Science, Osaka University, supported by MEXT Project for promoting public utilization of advanced research infrastructure (Program for supporting construction of core facilities) Grant Number JPMXS0441200024.

Notes and references

1 K. Schwab, E. A. Henriksen, J. M. Worlock and M. L. Roukes, Nature, 2000, **404**, 974–977.

2 X. Xu, L. F. C. Pereira, Y. Wang, J. Wu, K. Zhang, X. Zhao, S. Bae, T. C. Bui, R. Xie, J. T. L. Thong, B. H. Hong, K. P. Loh, D. Donadio, B. Li and B. Özyilmaz, Nat. Commun., 2014, **5**, 3689.

3 L. Cui, W. Jeong, S. Hur, M. Matt, J. C. Klöckner, F. Pauly, P. Nielaba, J. C. Cuevas, E. Meyhofer and P. Reddy, Science, 2017, **355**, 1192–1195.

4 A. Tavakoli, K. Lulla, T. Crozes, N. Mingo, E. Collin and O. Bourgeois, Nat. Commun., 2018, **9**, 4287.

5 R. Anufriev, S. Gluchko, S. Volz and M. Nomura, ACS Nano, 2018, **12**, 11928–11935.

6 Z. Zhang, Y. Ouyang, Y. Cheng, J. Chen, N. Li and G. Zhang, Phys. Rep., 2020, **860**, 1–26.

7 D. Polder and M. Van Hove, Phys. Rev. B, 1971, **4**, 3303.

8 E. Rousseau, A. Siria, G. Jourdan, S. Volz, F. Comin, J. Chevrier and J.-J. Greffet, Nat. Photonics, 2009, **3**, 514–517.

9 S. Shen, A. Narayanaswamy and G. Chen, Nano Lett., 2009, **9**, 2909–2913.

10 B. Song, Y. Ganjeh, S. Sadat, D. Thompson, A. Fiorino, V. Fernández-Hurtado, J. Feist, F. J. Garcia-Vidal, J. C. Cuevas, P. Reddy and E. Meyhofer, Nat. Nanotechnol., 2015, **10**, 253–258.

11 R. St-Gelais, L. Zhu, S. Fan and M. Lipson, Nat. Nanotechnol., 2016, **11**, 515–519.

12 H. Salihoglu, W. Nam, L. Traverso, M. Segovia, P. K. Venuthurumilli, W. Liu, Y. Wei, W. Li and X. Xu, Nano Lett., 2020, **20**, 6091–6096.

13 Y. D. Wilde, F. Formanek, R. Carminati, B. Gralak, P.-A. Lemoine, K. Joulain, J.-P. Mulet, Y. Chen and J.-J. Greffet, Nature, 2006, **444**, 740–743.

14 B. Guha, C. Otey, C. B. Poitras, S. Fan and M. Lipson, Nano Lett., 2012, **12**, 4546–4550.

15 E. A. Hawes, J. T. Hastings, C. Crofcheck and M. P. Mengüç, Opt. Lett., 2008, **33**, 1383–1385.

16 M. Laroche, R. Carminati and J.-J. Greffet, J. Appl. Phys., 2006, **100**, 063704.

17 K. Kim, B. Song, V. Fernández-Hurtado, W. Lee, W. Jeong, L. Cui, D. Thompson, J. Feist, M. T. H. Reid, F. J. García-Vidal, J. C. Cuevas, E. Meyhofer and P. Reddy, Nature, 2015, **528**, 387–391.

18 K. Kloppstech, N. Könne, S.-A. Biehs, A. W. Rodriguez, L. Worbes, D. Hellmann and A. Kittel, Nat. Commun., 2017, **8**, 14475.

19 L. Cui, W. Jeong, V. Fernández-Hurtado, J. Feist, F. J. García-Vidal, J. C. Cuevas, E. Meyhofer and P. Reddy, Nat. Commun., 2017, **8**, 14479.

20 Z.-Q. Zhang, J.-T. Lü and J.-S. Wang, Phys. Rev. B, 2018, **97**, 195450.

21 M. Prunnila and J. Meltaus, Phys. Rev. Lett., 2010, **105**, 125501.

22 V. Chiloyan, J. Garg, K. Esfarjani and G. Chen, Nat. Commun., 2015, **6**, 6755.

23 J. B. Pendry, K. Sasihithlu and R. V. Craster, Phys. Rev. B, 2016, **94**, 075414.

24 A. I. Volokitin, J. Phys.: Condens. Matter, 2020, **32**, 215001.

25 A. I. Volokitin, Phys. Rev. B, 2021, **103**, L041403.

26 T. Tokunaga, A. Jarzembski, T. Shiga, K. Park and M. Francoeur, Phys. Rev. B, 2021, **104**, 125404.

27 J. G. Simmons, J. Appl. Phys., 1963, **34**, 1793–1803.

28 P. Kim, L. Shi, A. Majumdar and P. L. McEuen, Phys. Rev. Lett., 2001, **87**, 215502.

29 L. Shi, D. Li, C. Yu, W. Jang, D. Kim, Z. Yao, P. Kim and A. Majumdar, J. Heat Transfer, 2003, **125**, 881–888.

30 D. Li, Y. Wu, P. Kim, L. Shi, P. Yang and A. Majumdar, Appl. Phys. Lett., 2003, **83**, 2934–2936.

31 A. I. Hochbaum, R. Chen, R. D. Delgado, W. Liang, E. C. Garnett, M. Najarian, A. Majumdar and P. Yang, Nature, 2008, **451**, 163–167.

32 J.-K. Yu, S. Mitrovic, D. Tham, J. Varghese and J. R. Heath, Nat. Nanotechnol., 2010, **5**, 718–721.

33 K. Hippalgaonkar, B. Huang, R. Chen, K. Sawyer, P. Ercius and A. Majumdar, Nano Lett., 2010, **10**, 4341–4348.

34 J. W. Roh, K. Hippalgaonkar, J. H. Ham, R. Chen, M. Z. Li, P. Ercius, A. Majumdar, W. Kim and W. Lee, ACS Nano, 2011, **5**, 3954–3960.

35 C.-L. Hsin, M. Wingert, C.-W. Huang, H. Guo, T.-J. Shih, J. Suh, K. Wang, J. Wu, W.-W. Wu and R. Chen, Nanoscale, 2013, **5**, 4669–4672.

36 R. Anufriev, Y. Wu and M. Nomura, J. Appl. Phys., 2021, **130**, 070903.

37 C. J. Muller, J. M. Van Ruitenbeek and L. J. De Jongh, Phys. C, 1992, **191**, 485–504.

38 R. Yamada, M. Noguchi and H. Tada, Appl. Phys. Lett., 2011, **98**, 053110.

39 D. Xiang, H. Jeong, T. Lee and D. Mayer, Adv. Mater., 2013, **25**, 4845–4867.

40 S. Sadat, E. Meyhofer and P. Reddy, Appl. Phys. Lett., 2013, **102**, 163110.

41 J. Zheng, M. C. Wingert, E. Dechaumphai and R. Chen, Rev. Sci. Instrum., 2013, **84**, 114901.

42 A. Weathers, K. Bi, M. T. Pettes and L. Shi, Rev. Sci. Instrum., 2013, **84**, 084903.

43 J. Y. Wu, W. Wu and M. T. Pettes, Rev. Sci. Instrum., 2016, **87**, 094901.

44 C. Cheng, W. Fan, J. Cao, S.-G. Ryu, J. Ji, C. P. Grigoropoulos and J. Wu, ACS Nano, 2011, **5**, 10102–10107.

45 R. Landauer, J. Phys.: Condens. Matter, 1989, **1**, 8099.

46 N. Agraït, J. G. Rodrigo and S. Vieira, Phys. Rev. B, 1993, **47**, 12345–12348.

Data Availability Statement:

The data supporting this article have been included as part of the Electronic Supplementary Information.